ACS APPLIED MATERIALS & INTERFACES

Research Article

www.acsami.org

High-Performance Composite Membrane with Enriched CO_2-philic Groups and Improved Adhesion at the Interface

Yifan Li,[†,‡] Shaofei Wang,[†,‡] Hong Wu,[†,‡] Ruili Guo,[§] Ye Liu,[†,‡] Zhongyi Jiang,*[,†,‡,§] Zhizhang Tian,[†,‡] Peng Zhang,[⊥] Xingzhong Cao,[⊥] and Baoyi Wang[⊥]

[†] Key Laboratory for Green Chemical Technology of Ministry of Education, School of Chemical Engineering and Technology, Tianjin University, Tianjin 300072, China

[‡] Collaborative Innovation Center of Chemical Science and Engineering, Tianjin 300072, China

[§] Key Laboratory for Green Process of Chemical Engineering of Xinjiang Bingtuan, School of Chemistry and Chemical Engineering, Shihezi University, Xinjiang, Shihezi 832003, China

[⊥] Key Laboratory of Nuclear Analysis Techniques, Institute of High Energy Physics, Chinese Academy of Sciences, Beijing 100049, China

Supporting Information

ABSTRACT: A novel strategy to design a high-performance composite membrane for CO_2 capture via coating a thin layer of water-swellable polymers (WSPs) onto a porous support with enriched CO_2-philic groups is demonstrated in this study. First, by employing a versatile platform technique combining non-solvent-induced phase separation and surface segregation, porous support membranes with abundant CO_2-philic ethylene oxide (EO) groups at the surface are successfully prepared. Second, a thin selective layer composed of Pebax MH 1657 is deposited onto the support membranes via dip coating. Because of the water-swellable characteristic of Pebax and the enriched EO groups at the interface, the composite membranes exhibit high CO_2 permeance above 1000 GPU with CO_2/N_2 selectivity above 40 at a humidified state (25 °C and 3 bar). By tuning the content of the PEO segment at the interface, the composite membranes can show either high CO_2 permeance up to 2420 GPU with moderate selectivity of 46.0 or high selectivity up to 109.6 with fairly good CO_2 permeance of 1275 GPU. Moreover, enrichment of the PEO segment at the interface significantly improves interfacial adhesion, as revealed by the T-peel test and positron annihilation spectroscopy measurement. In this way, the feasibility of designing WSP-based composite membranes by enriching CO_2-philic groups at the interface is validated. We hope our findings may pave a generic way to fabricate high-performance composite membranes for CO_2 capture using cost-effective materials and facile methods.

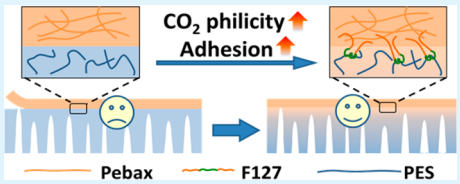

KEYWORDS: *composite membrane, interface, poly(ethylene oxide), surface segregation, CO_2 capture*

1. INTRODUCTION

Given the growing demands for energy-intensive lifestyles in the 21st century, the increasing amount of CO_2 emission from the combustion of fossil fuels has become a problem of global concern versus the sustainable development of human community.[1,2] Highly efficient CO_2 capture technologies with large capacity and low energy penalty are therefore urgently required, among which polymeric membrane-based technologies have possessed several advantages over other traditional technologies such as absorption and adsorption in capital investment, operational cost, and energy efficiency.[3−5] However, state-of-the-art polymeric gas separation membranes cannot guarantee the economic competitiveness of membrane technology because of their insufficiently high CO_2 permeance (mostly below 1000 GPU; 1 GPU = 10^{-6} cm^3 (STP) cm^{-2} s^{-1} $cmHg^{-1}$).[6,7] Because permeance is known as the quotient of permeability and membrane thickness, researchers are endeavored to pursue high-permeability polymeric membrane materials[8−11] or to reduce the membrane thickness without defects and mechanical instability.[12−15] A combined strategy of developing composite membranes comprising a thin film of a high-permeability material and a porous support is therefore of great importance,[16,17] while the feasibility of thin-film fabrication is often neglected in the development of new membrane materials.

In recent years, water-swellable polymers (WSPs) have aroused significant research interest as highly permeable membrane materials for CO_2 separation.[11,18] First, water often exists in many CO_2-containing industrial gases.[6,19,20] It has negative effects on conventional glassy polymer membranes because of the completive sorption effect and consequent blockage of the gas-permeation route,[21,22] while it plays positive roles in WSP membranes because of membrane swelling and the fast selective transport of other forms of CO_2 (e.g., HCO_3^-).[23,24] Second, defect-free thin films of WSP can be simply deposited onto a porous support for composite

Received: January 17, 2014
Accepted: April 15, 2014
Published: April 15, 2014

membranes by dip coating or interfacial polymerization.[24,25] Last but not least, a large number of WSPs [e.g., poly(vinyl alcohol),[26] chitosan,[27] and Pebax[28]] are usually of low price and easily available and have excellent film-forming ability and mechanical stability. Consequently, WSPs combine the advantages of high CO_2 separation performance and the fascinating feasibility of large-scale fabrication of composite membranes.

For high-permeance composite membranes based on WSPs, the thickness of the selective layer is usually below 1 μm, and hence the interface between the selective and support layers can significantly affect the flexibility and packing manner of polymer chains confined in such a narrow space.[29] Most importantly, when the selective layer is excessively swollen by water, it will often be detached from the neighboring support layer because of the external interfacial tension.[30] Therefore, the interfacial adhesion between the adjacent layers should be strong enough to prevent the selective layer from peeling off. According to adhesive principles based on adsorption theory,[31] enriching polar groups at the interface is beneficial to adequate interfacial adhesion. On the other hand, polar groups can preferentially interact with CO_2 via dipole−quadrupole interactions.[32] Because of the extremely thin selective layer of composite membranes, the polar groups at the interface zone are expected to significantly affect the membrane performance by enhancing selective CO_2 sorption. Although abundant polar groups are known to cause high cohesive energy and a low fraction of free volume,[33] the effect of swelling mediated by water delicately solves this problem. In summary, a versatile method to modify the surface of the support layer with polar groups is expected toenhance both interlayer interactions and selective CO_2 sorption within the interfacial zone. To the best of our knowledge, rare efforts have been devoted to enhancing the CO_2 capture performance of composite membranes by surface modification of the support layer.

In this study, a high-performance composite membrane for CO_2 capture was designed and fabricated by modifying the surface of the support layer with EO groups. A widely utilized platform technique combining non-solvent-induced phase separation and surface segregation was employed to fabricate porous support membranes with abundant CO_2-philic EO groups at the surface.[34,35] Specifically, a series of support membranes were fabricated by surface segregation of Pluronic F127 (abbreviated as F127 in the following text) during the non-solvent-induced phase inversion of poly(ether sulfone) (PES). In this way, poly(ethylene oxide) (PEO) segment of F127 was enriched at the surface of support membranes and also at the interface of the corresponding composite membranes. Pebax MH 1657 (abbreviated as Pebax in the following text) was selected as the selective layer material because of its low price, good film-forming ability, and high CO_2 permeability in the presence of water.[28] Furthermore, Pebax as a PEO-based copolymer possesses the same structural unit (PEO) as F127, which is favorable for improving the compatibility of the adjacent layers. The as-prepared composite membranes exhibit high CO_2 permeance, high CO_2/N_2 selectivity, and high stability under a humidified state. The interfacial adhesion strength was evaluated by T-peel tests. The correlation between the interfacial structures and separation performance was explored by positron annihilation spectroscopy (PAS).

2. EXPERIMENTAL METHODS

2.1. Materials. PES (6020P, M_w = 29000) was purchased from BASF Co. (Ludwigshafen, Germany) and dried at a temperature of 110 °C for 12 h before use. Pebax 1657 and F127 were purchased from Arkema (Paris, France) and Sigma-Aldrich, respectively. The chemical structures of PES, F127, and Pebax 1657 are shown in Scheme 1. *N*-Methyl-2-pyrrolidinone (NMP), ethanol, and *n*-heptane

Scheme 1. Chemical Structures of (a) PES, (b) Pluronic F127, and (c) Pebax 1657

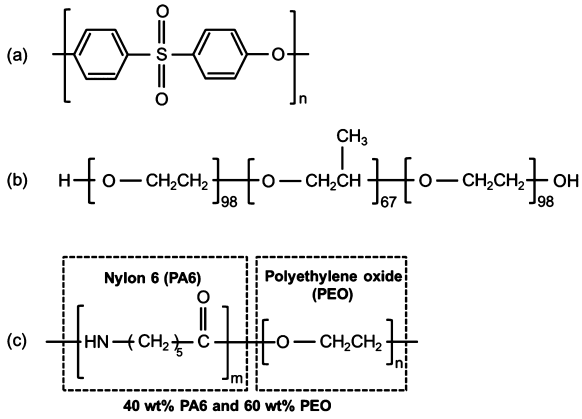

were purchased from Tianjin Guangfu Fine Chemical Research Institute (Tianjin, China). All chemicals were of reagent grade or higher and were used without further purification.

2.2. Preparation of Support Membranes. Casting solutions were prepared by dissolving PES and a certain amount of F127 into NMP (containing ethanol as a nonsolvent additive) under mechanical stirring at 60 °C for 4 h. The compositions of the casting solutions are shown in Table 1 (including the corresponding abbreviation of each

Table 1. Chemical Composition of the Casting Solutions of Support Membranes

sample	PES (g)	F127 (g)	NMP (g)	ethanol (g)	total (g)	W_{127}/W_{PES} (%)[a]
PES	3.00		9.00	1.50	13.50	0
PES−F127(5)	3.00	0.15	8.85	1.50	13.50	5
PES−F127(10)	3.00	0.30	8.70	1.50	13.50	10
PES−F127(15)	3.00	0.45	8.55	1.50	13.50	15
PES−F127(20)	3.00	0.60	8.40	1.50	13.50	20
PES−F127(30)	3.00	0.90	8.10	1.50	13.50	30

[a]The weight ratio of Pluronic F127 to PES in the casting solution.

membrane). The homogeneous solutions were kept without stirring overnight to ensure the complete release of bubbles. When cooled to room temperature, the solutions were cast onto a glass substrate with a steel knife, and the wet thickness of the nascent membranes was controlled at about 240 μm. The nonsolvent was allowed to evaporate for 30 s, and then the nascent membranes together with the glass substrates were immersed into a coagulation bath of deionized water at 27 ± 1 °C. When the membranes were solidified and peeled off from the substrate, it was subsequently washed with deionized water to completely remove the residual solvent and F127. Then a two-step solvent-exchange procedure was conducted by immersing the wet membranes in three ethanol baths for 2 h each, followed by immersion in three *n*-heptane baths for 2 h each. The resultant membranes were dried and kept at 30 °C and 40% relative humidity (RH) before use.

2.3. Preparation of Composite Membranes. Pebax was dissolved in ethanol/water (70/30 wt %) with stirring and reflux at 80 °C to obtain a homogeneous solution. The concentration of Pebax

Table 2. XPS Analysis, Water Contact Angle, Thickness, and Pore Size of Support Membranes

	membrane surface composition (mol %)[a]									
	C				surface coverage of the PEO segment (%)			thickness (μm)		
sample	C−C	C−O[b]	O	S	exp.[c]	cal.[c,d]	contact angle (deg)	exp.[c]	cal.[c,e]	pore size (nm)
PES	48.4	24.1	24.0	3.9	0	0	62.5 ± 1.8	171 ± 10		4−11
PES−F127(5)	46.4	26.5	23.9	3.8	5.18 ± 0.45	2.78 ± 0.33	58.9 ± 1.5	189 ± 9	189 ± 1	5−15
PES−F127(10)	44.0	29.4	23.7	3.6	11.34 ± 1.01	5.44 ± 0.89	54.4 ± 1.6	200 ± 5	200 ± 2	6−14
PES−F127(15)	41.1	32.7	23.6	3.4	18.55 ± 1.24	8.04 ± 1.01	50.5 ± 1.4	219 ± 13	218 ± 5	6−16
PES−F127(20)	39.0	35.3	23.4	3.1	23.94 ± 1.73	10.59 ± 1.46	46.9 ± 1.8	230 ± 8	227 ± 3	8−21
PES−F127(30)	36.2	38.5	23.2	2.9	30.66 ± 1.38	15.51 ± 1.53	41.9 ± 1.2	231 ± 7	225 ± 2	10−20

[a]The error limits are within 5%. [b]"C−O" stands for ether carbon, which actually consists of carbon atoms in the C−O and C−S bonds. [c]"Exp." and "Cal." stand for experimental and calculated values, respectively. [d]The calculated values of the surface coverage of PEO can be obtained by evaluating the membrane surface composition based on the composition of the casting solution. [e]The theoretical thickness of PES−F127(X) is calculated by a "mixed-matrix" model using the measured density of the PES membrane as the density of the PES matrix.

was controlled at 3 wt %, except when the effect of the Pebax concentration was studied. Composite membranes were prepared by casting a Pebax solution onto support membranes at room temperature, and then the residual casting solution was removed by slowly increasing the gradient of the membrane surface up to 30°. The resultant composite membranes were kept at 30 °C and 40% RH to allow the residual solvent to evaporate.

2.4. Membrane Characterization. The cross-sectional morphologies of support and composite membranes were characterized by using field-emission scanning electron microscopy (FESEM; Nanosem 430) operating at 10 kV. The chemical structure of the membrane was characterized by a Nicolet-560 Fourier transform infrared (FT-IR) spectrometer with a scan range of 4000−400 cm^{-1}. The static contact angles were measured using a contact-angle goniometer (JC2000C Contact Angle Meter, Powereach Co., Shanghai, China). The chemical composition of the membrane surface was determined using X-ray photoelectron spectroscopy (XPS; PHI-1600 X-ray photoelectron spectrometer) using Mg Kα as the radiation source. The takeoff angle of the photoelectron was set at 90°. Survey spectra of membranes were collected over a range of 0−1100 eV. The pore size of the support membranes was estimated following a method previously reported,[36] based on liquid−liquid displacement porosimetry experiments proposed by Zydney and co-workers.[37] The interlayer adhesion strength of the composite membranes was measured by the T-peel test, using a Micro-Uniaxial Fatigue Testing system (MUT-1020, CMC). The size of sample was 8 mm (width) × 30 mm (length). The displacement-dependent load curves were recorded with a loading rate of 0.5 mm s^{-1} at room temperature. The free volume property at the interface was measured by Doppler broadening PAS in a ^{22}Na slow positron beamline, using one high-purity germanium detector. Slow positrons in the energy range of 0.18−20 keV were implanted into the specimens. Each spectrum was collected with total counts of about 5×10^5 and characterized by the S parameters.

2.5. Gas-Permeation Experiments. Single CO_2 and N_2 and binary CO_2−N_2 (10 vol %/90 vol %) gas-permeation experiments were conducted at 25 °C based on the conventional constant pressure/variable volume technique (a scheme of the apparatus is shown in Figure S1 in the Supporting Information, SI). CH_4 was selected as the sweep gas to determine the permeability of CO_2 and N_2. In a typical measurement, 3 bar of feed gas was first introduced into a water bottle (35 °C) to be saturated with water vapor and then passed through an empty bottle to remove the residual water. Meanwhile, the sweep gas was humidified at room temperature. The RH values for the feed and sweep gases were 82 ± 5% and 89 ± 4%, respectively. The flow rate and composition of the sweep gas were recorded every 5 min until they no longer varied with time. The feed and sweep gases could also be directly introduced into the membrane cell to conduct a dry-state gas-permeation test.

The compositions of the feed, retentate, and permeate were measured using gas chromatography (Agilent 6820). The permeance (P/l, GPU) of either gas was obtained from the average value of at least two tests, by using eq 1:

$$(P/l)_i = \frac{Q_i}{\Delta p_i A} \tag{1}$$

where Q_i is the volumetric flow rate of gas i (cm^3 s^{-1}) at standard temperature and pressure (STP), Δp_i is the transmembrane partial pressure difference of gas i (cmHg), and A is the effective membrane area (12.56 cm^2). The pure-gas or mixed-gas selectivity (α_{ij}) was calculated by eq 2:

$$\alpha_{ij} = \frac{(P/l)_i}{(P/l)_j} \tag{2}$$

RESULTS AND DISCUSSION

3.1. Structures and Properties of Support Membranes. The thickness of each support membrane is obtained from FESEM images (Figure S2 in the SI) and shown in Table 2. With an increase of the F127 content, the thickness of the support membrane increases from 171 μm (PES) to 231 μm [PES−F127(30)]. The increment of the membrane thickness is attributed to the increment of the total mass (PES + F127). For example, as shown in Table 2, the theoretical thicknesses of PES−F127(15) and PES−F127(30) should have been around 198−201 and 224−227 μm, respectively, which are close to their experimental values (200 and 231 μm). Although some F127 molecules may release into the coagulation bath during and after the coagulation process, the coagulation process is so fast that it "freezes" the framework of the membrane.[34] Consequently, the release of F127 leads to an increase of the membrane porosity rather than a collapse of the "frozen" membrane framework. From these facts, it can be inferred that the contrast (or physical aging) of the membrane during drying and storage is not obvious, which should mainly be attributed to the solvent-exchange treatment.

The chemical structures of support membranes are qualitatively depicted in FT-IR spectra (see Figure S4 in the SI) and quantitatively revealed by XPS analysis (Table 2). The surface coverage of the PEO segment is calculated by a method described in the SI. It is shown in Table 2 that the experimental values are apparently higher than the theoretical values for the same membrane, indicating surface segregation of the PEO segment.[34] That is, because of the difference in the hydrophilicity between PEO and PES, the hydrophilic PEO chain of F127 is prone to spontaneously migrating toward water

coagulation during the phase separation process rather than remaining within the hydrophobic matrix of PES. On the other hand, the relatively hydrophobic poly(propylene oxide) (PPO) chain of F127 serves as an "anchor" to prevent excessive release of F127 into coagulation. In this way, F127 is enriched at the membrane surface, and the surface coverage of PEO (the experimental value) is higher than that in the bulk (the calculated value). As the content of F127 increases from 0 to 30%, the surface coverage of the PEO segment increases from 0 to 30.66%, and simultaneously the contact angle of the membrane surface decreases from 62.5° to 41.9° (Table 2). The improvement of the hydrophilicity of the membrane surface is attributed to surface enrichment of the PEO segment.

Table 2 also shows the average pore size of support membranes, which helps one to understand the process of surface segregation in this study. The pore size can also be estimated by FESEM images (Figure S3 in the SI). In our previous study, the dual role of F127 as both surface modifier and pore-forming agent was investigated.[38] Some F127 molecules are prone to segregate to the membrane/water interface because of the presence of hydrophilic PEO blocks, while the hydrophobic PPO blocks of F127 are bound to and/or tangled with PES chains, preventing the release of F127; the excessive amount of F127 can self-assemble into core/shell-structured spherical micelles, which act as "templates" for mesopore generation when extracted into the coagulation bath. In the present study, the role of a pore-forming agent can be directly verified by the increment of the pore size with an increase of the F127 content. At higher concentration, F127 is more prone to assemble into micelles. In particular, the mean pore size of the membranes for PES−F127(20) and PES−F127(30) is apparently larger than that of other membranes, indicating that F127 mainly exists in the form of micelles rather than stretched chains during and after the coagulation process.

Pure-gas-permeation tests were conducted to provide more information about the membrane structures and properties. Because of the absence of a pore-forming agent, the PES support membrane displays rather low CO_2 permeance (1542 GPU) at the dry state. When the membrane is tested at a humidified state, CO_2 permeance is recovered up to 4850 GPU, which may be attributed to the partial recovery of a collapsed membrane pore and the water-induced plasticization effect. With the content of F127 increasing, CO_2 permeance of a dry-state membrane gradually increases, and a notable "jump" of CO_2 permeance is observed when the F127 content increases from 15% to 20% (Figure 1), which supports the hypothesis that a large amount of F127 micelles forms during the formation of PES−F127(20) and PES−F127(30). More interestingly, the improvement of CO_2 permeance caused by humidification becomes more and more significant with the increment of the F127 content, which is desired for a low-resistance support membrane. It is inferred that F127 containing hydrophilic PEO chains more easily adsorbs water and becomes swollen than hydrophobic PES.

When the selectivity data shown in Figure 1 are combined, the transport mechanisms of the membranes can be clearly depicted, which is important to better understand the structures of the support membranes. At a dry state, the ideal CO_2/N_2 selectivity of PES lies above 1, suggesting that the skin district of the membrane becomes partially densified. In this case, both the solution−diffusion and Knudsen diffusion mechanisms occur. When the F127 content increases from 0 to 15%, the CO_2/N_2 selectivity rapidly falls below 0.9, indicating that

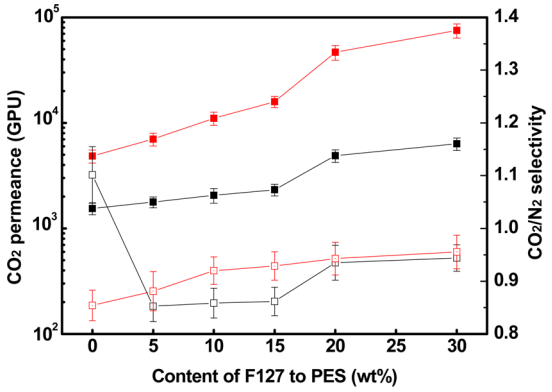

Figure 1. Pure-gas CO_2 permeance (solid symbol) and CO_2/N_2 selectivity (open symbol) of support membranes at dry (black line) and humidified (red line) conditions (temperature, 25 °C; feed pressure, 3 bar).

Knudsen diffusion becomes the dominant transport mechanism (the Knudsen selectivity for CO_2/N_2 is about 0.8). When the F127 content increases from 15% to 30%, the CO_2/N_2 selectivity gradually increases up to 0.93. When the "jumps" of CO_2 permeance in Figure 1 are combined, herein the dominate transport mechanism changes from Knudsen diffusion to viscous flow (the viscous-flow selectivity for CO_2/N_2 is 1). At a humidified state, all membranes except PES and PES−F127(5) exhibit CO_2/N_2 selectivity between 0.9 and 1, and it monotonically increases with the F127 content. These facts demonstrate that viscous flow dominates the gas transport behaviors within humidified membranes.

3.2. Structures and Properties of Composite Membranes. The high-resolution images of composite membranes are shown in Figure S5 in the SI. For each sample, a homogeneous selective layer with uniform thickness is deposited on the support membrane, and no visible interfacial defect is observed. The thickness of the selective layer is 268 ± 3 nm for Pebax/PES, Pebax/PES−F127(15), and Pebax/PES−F127(30), indicative of the weak dependence of the thin-film thickness on the surface modification.

The effect of the surface modification of the support membrane on the interlayer adhesion strength is evaluated by the T-peel test. Figure 2a shows the load versus displacement curve of dry-state composite membranes. When the F127 content increases from 0 to 15%, the peeling strength increases from 1.0 to 1.4 N, and the corresponding peeling-off displacement decreases from 10 to 4 mm. Consequently, enrichment of the PEO segment enhances the adhesion strength between the adjacent layers. In order to investigate the effect of moisture within the membrane on the interlayer adhesion strength, the membranes that have been previously humidified in 100% RH for 48 h are tested for a further comparison (Figure 2b). Surprisingly, the selective layer of Pebax/PES is suddenly peeled off when the displacement increases up to 4.3 mm. As a consequence, the test has to be interrupted at this point. This fact indicates that the presence of water significantly decreases the interlayer adhesion strength, and at some place, the adjacent layers are separated from each other. By comparison, the highest peeling strength for Pebax/PES−F127(15) is 0.8 N, and the curve appears to be quite smooth. As such, Pebax/PES−F127(15) shows greater advantages over Pebax/PES at a humidified state than a dry

dx.doi.org/10.1021/am500356g | ACS Appl. Mater. Interfaces 2014, 6, 6654−6663

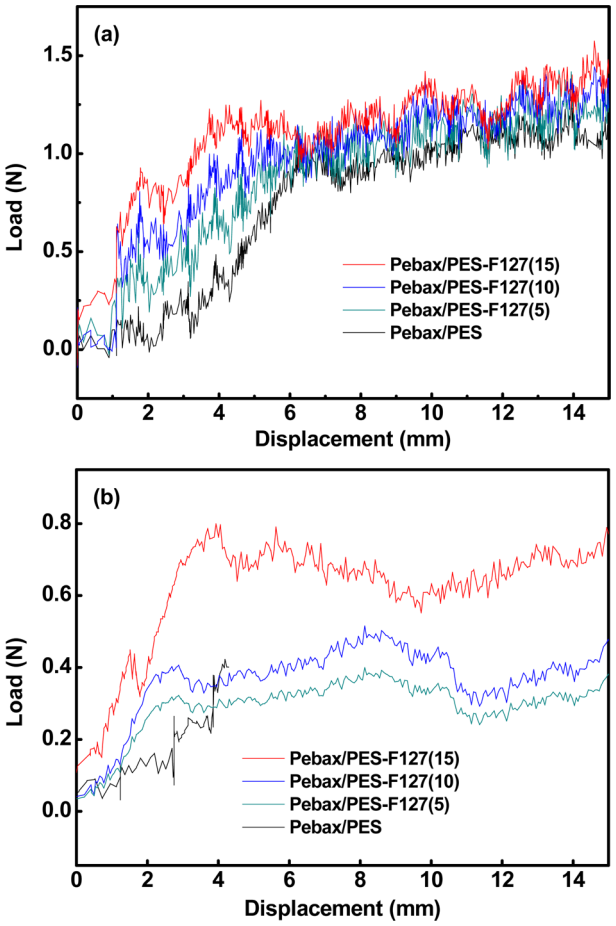

Figure 2. T-peel load versus displacement curves for composite membranes: (a) at a dry state; (b) at a humidified state.

state, although the interlayer adhesion strength of a humidified-state membrane is weaker than that of a dry-state membrane.

For Pebax/PES−F127(20) and Pebax/PES−F127(30), the T-peel curve shows a rapid ascent first (as shown in Figure S6 in the SI), followed by a sudden break because of rupture of the active layer. The rapid increase of the load further illustrates that the PEO segments at the interface can lead to enhanced adhesion strength. The sudden fracture of the active layer demonstrates that the cohesive force of the active layer cannot afford the peeling force. Although more PEO segments are enriched at the interface, serious pore intrusion may prevent perfect coverage of the active layer onto the support layer, which may be detrimental to the cohesive strength of the active layer. Notably, at a humidified state, the breaking load of Pebax/PES−F127(30) has already approached the peeling strength of Pebax/PES−F127(15), which indicates the effect of water-induced plasticization and reduced inner stress.

To probe the interfacial structure at the angstrom level, variable-energy PAS (VEPAS) is used by implanting positrons to the specimens with moderate energy, and the depth profile of free volume can be evaluated by the *S* parameter. The mean implantation depth (nm) of the energetic positrons is expressed by eq 3:

$$\bar{Z} = \left(\frac{40}{\rho}\right)E^{1.6} \tag{3}$$

where E is the positron incident energy (keV) and ρ is the density (g/cm^3) of the materials. The S−E curves of support membranes are provided in Figure S7 in the SI, which verifies the role of F127 as a pore-forming agent during the phase-inversion process. For composite membranes, the position of the interface is determined according to the thickness of the selective layer (about 270 nm). As shown in Figure 3, when the

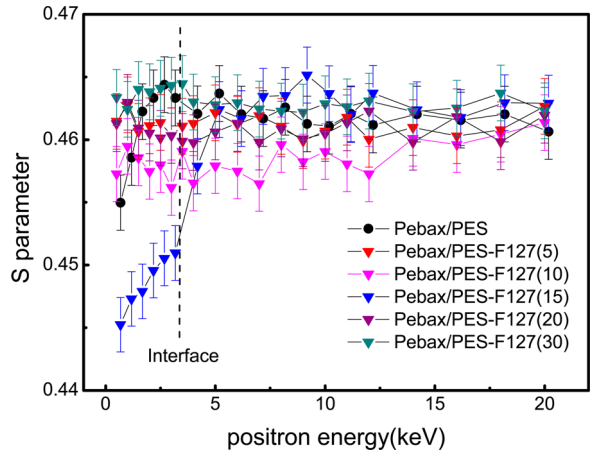

Figure 3. *S* parameter as a function of the incident positron for composite membranes.

F127 content increases from 0 to 15%, the *S* parameter at the interface decreases, supporting the role of interfacially enriched PEO segments in improving the interlayer adhesion. When the F127 content increases from 15% to 30%, the *S* parameter at the interface increases again. This can be interpreted by the relatively larger pores for PES−F127(20) and PES−F127(30), where serious pore intrusion may occur and hinder formation of the perfect active layer, as revealed by the T-peel test. More importantly, a sharp variation of the *S* parameter near the interfacial zone is observed for Pebax/PES−F127(15), while similar results are not observed for other membranes. These facts indicate that the interface of Pebax/PES−F127(15) is quite different from that of other membranes: because PAS measurements have to be conducted free of moisture, the necessary vacuum drying may further result in dewetting of the active layer and produce new defects. From the shape of the curves of all samples, we can infer that it is only Pebax/PES−F127(15) that does not suffer from the dewetting process during pretreatment of the PAS samples. The unique interfacial adhesion of Pebax/PES−F127(15) can be interpreted from two aspects: (1) abundant PEO segments guarantee the interfacial compatibility; (2) a proper degree of pore intrusion can prevent the dewetting process. Because of the confined nanospace within the surface pores of support membranes, the Pebax chains within the pores display lower mobility, which is known as "chain rigidification". As a matter of fact, chain rigidification caused by pore intrusion has been observed in the literature, which usually causes a decrease of flux and an increase of selectivity.[39−41] Considering that the interactions between Pebax and the PEO segment are actually not strong,[42−44] the contribution of chain rigidification resulting from pore intrusion becomes very important to ensure adequate interfacial adhesion. For Pebax/PES−F127(20) and Pebax/PES−F127(30), the F127 micelles cause too large pore sizes of support membranes to create the desired confined space but produce undesired pinholes near the pores.

The gas-permeation properties of dry-state composite membranes are plotted in Figure 4a. The minimum CO_2

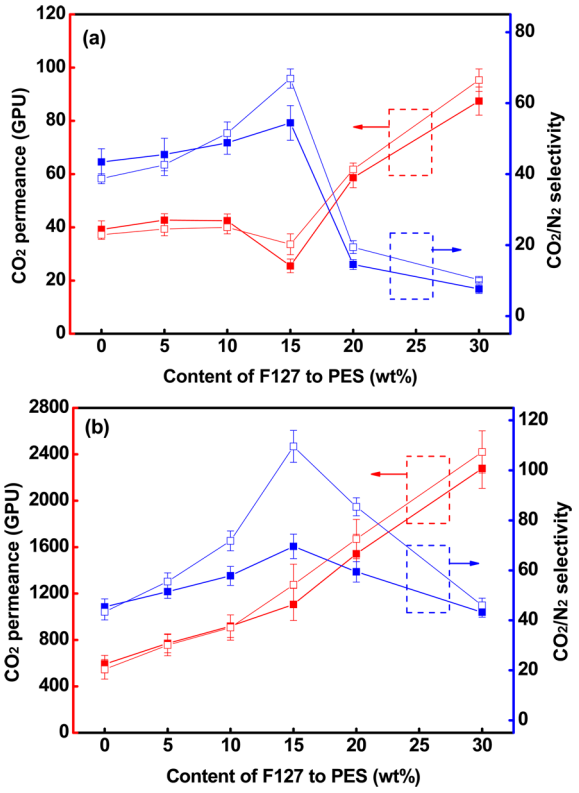

Figure 4. Pure-gas (solid symbol) and mixed-gas (open symbol) permeation properties of composite membranes: (a) dry membranes; (b) humidified membranes (25 °C and 3 bar).

permeance and maximum selectivity are observed for Pebax/PES−F127(15), which can be predicted by the PAS results. The rapid increase of CO_2 permeance and decrease of the selectivity at higher F127 content confirms the existence of defects. Once the dry-state membrane is pressed, the selective layer is prone to being partially damaged, and new defects are expected to appear. Interestingly and surprisingly, in the presence of F127, the mixed-gas selectivity becomes higher than the pure-gas selectivity. A similar phenomenon has been found when the overwhelming adsorption of CO_2 extruded the adsorption of N_2.[8] The largest difference between the mixed-gas and pure-gas selectivities was also found at the F127 content of 15%, which implies that the interfacial adhesion may affect the adsorption of gases: good interfacial adhesion can lower the mobility of the PEO chains at the interface, which further extrudes N_2 permeation. When the F127 content increases above 20%, the large pore of support membranes cannot guarantee a defect-free active layer, and the benefit of preferential CO_2 adsorption is not obvious. Consequently, it is reasonable to assume that enrichment of the CO_2-philic groups at the interface increases the solubility selectivity of the membrane.

By comparison, composite membranes exhibit much better performance at a humidified state. CO_2/N_2 selectivity increases when the F127 content increases from 0 to 15%, and the highest value (109.6) is achieved for Pebax/PES−F127(15). This value is obviously higher than the intrinsic ideal CO_2/N_2 selectivity of Pebax (about 50−55), and similar results were also reported elsewhere.[45] The unusually high CO_2/N_2 selectivity can be attributed to interfacially enriched PEO and water-facilitated CO_2 transport. The role of interfacially enriched PEO in enhancing the solubility selectivity has been discussed previously. By testing the membranes at 50 °C, a large decrease of the selectivity is observed (Figure S8 in the SI), demonstrating that the membrane selectivity is mainly determined by the solubility selectivity. Water-facilitated CO_2 transport can be seen by comparing parts a and b of Figure 4 because Figure 4b shows a larger difference between the mixed-gas and pure-gas selectivities than Figure 4a. Figure 4b shows much higher CO_2/N_2 selectivity than Figure 4b at high F127 content, indicating that water can plasticize Pebax chains, fill in the defects, and promote self-healing of the active layer.

Another interesting finding is about the trend of CO_2 permeance for humidified composite membranes. Although the maximum CO_2/N_2 selectivity is observed for Pebax/PES−F127(15), CO_2 permeance monotonically increases with the increment of the F127 content. Again, a comparison between parts a and b of Figure 4 implies the important role of water. To better illustrate this phenomenon, the performance of a dense Pebax membrane and a Pebax-F127(15) blend membrane is measured. It is observed in our experiment that the addition of 15 wt % F127 into Pebax leads to a ∼20% decrease of the CO_2 permeability at the dry state, which should be ascribed to the crystalline tendency of the long PEO segment (4.41 kg/mol) in F127. However, the CO_2 permeability of a Pebax-F127(15) blend membrane is comparable to that of a Pebax membrane at a humidified state, indicating that water has disrupted the crystallinity of PEO and that the higher content of PEO in a Pebax-F127(15) blend membrane leads to higher CO_2 solubility.[46,47] For Pebax/PES−F127 membranes, the selective layer is very thin, and hence the interfacial zone rich in PEO segments can also significantly affect the overall separation performance. Considering surface segregation of the PEO segment at the interface, the positive role of F127 in enhancing the CO_2 solubility becomes predominant, and therefore CO_2 permeance increased with the F127 content. On the other hand, the lowered mass-transfer resistance of the support layer contributes to the decrease of the overall resistance, especially for composite membranes with low-permeance support layers. In this way, CO_2 permeance and CO_2/N_2 selectivity simultaneously increase when the F127 content is not higher than 15%. For Pebax/PES−F127(20) and Pebax/PES−F127(30), the expected defects resulting from insufficient mechanical strength of the selective layer further increase CO_2 permeance at the cost of CO_2/N_2 selectivity.

Membrane stability against liquid water is also useful to illustrate the interfaical adhesion strength of a composite membrane. For any composite membrane, a hydrophilic selective layer is prone to swelling by water. When water is adsorbed into the selective layer from wet gas, a gradual increase of water uptake and a homogeneous distribution of the adsorbed water can be expected. In this case, excessive swelling will not occur locally. However, when the selective layer directly contacts liquid water, the locally concentrated water molecules cannot be evenly distributed rapidly, which will lead to excessive swelling. Actually, the fact that liquid water is detrimental to the interfacial stability of a composite membrane has been widely recognized in the field of pervaporation.[48,49] In this study, with the purpose of evaluating the stability of a membrane against liquid water, 2 mL of deionized water is

dx.doi.org/10.1021/am500356g | ACS Appl. Mater. Interfaces 2014, 6, 6654−6663

sprayed onto the surface of composite membranes. The surface-wetted membranes are then sealed in the membrane cell for gas separation measurement. As shown in Figure 5, Pebax/PES

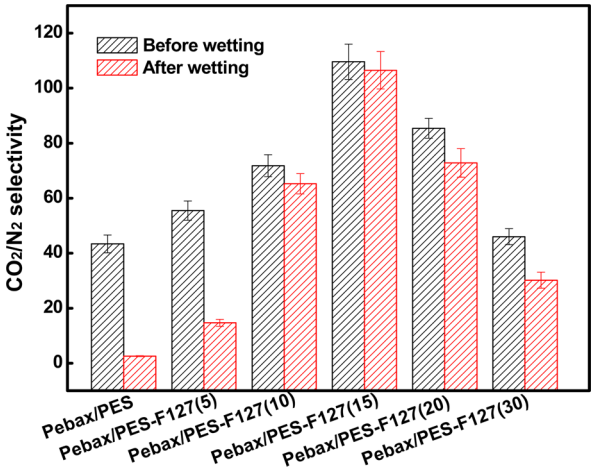

Figure 5. Effect of surface wetting on the selectivities of composite membranes (25 °C and 3 bar).

loses its separation capacity after surface wetting, implying the damage of the selective layer by liquid water. In sharp contrast, Pebax/PES−F127(15) shows almost the same selectivity as the value obtained before surface wetting. These results can be interpreted by the improved interfacial adhesion: because the F127-modified support membrane can reduce the hydrophilicity difference of adjacent layers and therefore enhance the interfacial adhesion strength, the stress at the interface due to the high degree of swelling can be reduced. For Peba/PES−F127(15), moderate pore intrusion restricts the chain mobility of Pebax and therefore further enhances the interfacial stability. The contribution of pore intrusion to the interfacial adhesion of a composite membrane has been reported elsewhere.[50] It is also notable that the performance of Pebax/PES−F127(15) under a 100 h long-term gas separation experiment remains almost unchanged (Figure S9 in the SI). Obviously, a thin-film Pebax membrane is not stable in the presence of liquid water because of excessive swelling, while it is the improved interlayer adhesion that prevents the selective layer of Pebax from deterioration.

When the experimental results in this study and our previous studies about interfacial stability are summarized,[30,41,51,52] it is concluded that the desired interface structure of a WSP-based composite membrane for CO_2 capture should satisfy three requirements: (1) the surface of the support layer should be hydrophilic enough to ensure compatibility between two layers; (2) a proper pore size of the support layer is required for appropriate pore intrusion, which is crucial to guaranteeing a highly stable interface; (3) the functional groups at the surface of the support layer are more capable of enabling preferential CO_2 adsorption.

The effect of the Pebax concentration in the coating solution is shown in Figure 6. Because the Pebax concentration mainly determines the active layer thickness, this figure is replotted versus the thickness of the active layer. CO_2 permeance decreases with the increment of the active layer thickness, while CO_2/N_2 selectivity increases. Such a tendency can be interpreted by the increase of the membrane compactness. Figure 6 also allows us to select the appropriate concentration

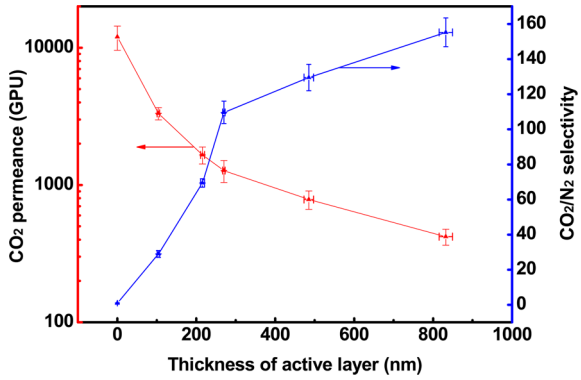

Figure 6. Effect of the active layer thickness on the CO_2 capture properties of Pebax/PES−F127(15). The thickness is tuned by fixing the Pebax concentration in the casting solution at 0, 1%, 2%, 3%, 4%, and 5%, respectively, from the left to right sides (25 °C and 3 bar).

of the coating solution, according to application requirements. For example, the membrane prepared using a 1% Pebax solution exhibits high CO_2 permeance (3323 GPU) and moderate CO_2/N_2 selectivity (28.9), while the membrane prepared using a 4% Pebax solution exhibits moderate CO_2 permeance (784 GPU) and high CO_2/N_2 selectivity (130). Although the former membrane is favored according to the viewpoint of Merkel et al.,[6] the latter membrane may also be useful when high CO_2 purity is required.[7]

The effect of the feed pressure is shown in Figure 7. Unlike facilitated transport membranes, the membranes fabricated in

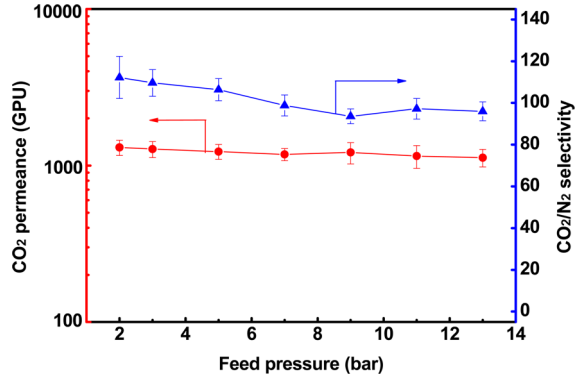

Figure 7. Effect of the operating pressure on the CO_2 capture properties of Pebax/PES−F127(15) (25 °C).

this study do not show remarkable decrement of CO_2 permeance and CO_2/N_2 selectivity with the increment of the feed pressure, indicating that the separation performance of Pebax does not rely much on the facilitated transport mechanism. Although a slight decrease of CO_2 permeance and CO_2/N_2 selectivity along with the feed pressure is observed, CO_2 permeance higher than 1000 GPU with CO_2/N_2 selectivity higher than 90 is maintained in the whole range of feed pressure.

3.3. Comparison with Other Composite Membranes and Asymmetric Membranes. The CO_2 capture performances of some representative composite membranes and asymmetric membranes are summarized in Table 3. Obviously, the membranes with WSP-selective layers exhibit superior CO_2 capture performance under humidified conditions. With no doubt, this type of CO_2 capture membrane should be paid

dx.doi.org/10.1021/am500356g | ACS Appl. Mater. Interfaces 2014, 6, 6654−6663

Table 3. Comparison of the Membrane Separation Properties of Other Composite Membranes and Asymmetric Membranes with the Current Work

membrane	CO_2 permeance (GPU)	CO_2/N_2 selectivity[a]	testing conditions	ref
PIM-1−Matrimid (asymmetric)	212.4	24.5	pure gas, RT, 2 bar, dry membrane	12
Utem−ZIF-8 (asymmetric)	26	36	mixed gas (20 vol % CO_2), 35 °C, 100 psia, dry membrane	53
PSf−carbon xerogel (asymmetric)	95.4	43.6	pure gas, RT, 5 bar, dry membrane	54
Pebax−PEG/PAN	93[b]	70[b]	mixed gas (25 vol % CO_2), 20 °C, 8 bar, dry membrane	45
PDMAEMA−PEGMEMA/PSf	30	31	25 °C, 1 bar, humidified membrane	55
PVAm/PPO	440	183	mixed gas (10 vol % CO_2), 25 °C, 5 bar, humidified membrane	14
Polaris	1000	50	not provided	6
polyactive/PDMS/PAN	2330[b]	30	pure gas, 60 °C, 1 bar, dry membrane	16
	5000[c]	30	pure gas, 60 °C, 1 bar, humidified membrane	17
	925[b]	55[b]	mixed gas (15 vol % CO_2), 20 °C, 5 bar, dry membrane	16
DAmBS−DGBAmE−TMC/PDMS/PSf	5830	86	mixed gas (15 vol % CO_2), 25 °C, 1.1 bar, humidified membrane	25
	2000[b]	30[b]	mixed gas (15 vol % CO_2), 25 °C, 5 bar, humidified membrane	
DNMDAm−DGBAmE−TMC/PDMS/PSf	1600	138	mixed gas (15 vol % CO_2), 25 °C, 1.1 bar, humidified membrane	5
	650[b]	65[b]	mixed gas (15 vol % CO_2), 25 °C, 5 bar, humidified membrane	
PVAm−PIP/PSf	6500	277	mixed gas (15 vol % CO_2), 25 °C, 1.1 bar, humidified membrane	24
	3690[b]	85[b]	mixed gas (15 vol % CO_2), 25 °C, 6 bar, humidified membrane	
Pebax/PES−F127(15)	1275	109.6	mixed gas (10 vol % CO_2), 25 °C, 3 bar, humidified membrane	this work
	1228	106.4	mixed gas (10 vol % CO_2), 25 °C, 5 bar, humidified membrane	this work
Pebax/PES−F127(20)	1670	85.4	mixed gas (10 vol % CO_2), 25 °C, 3 bar, humidified membrane	this work

[a]The values were mostly calculated as the ratio of CO_2 permeance to N_2 permeance. [b]Values are approximated from plots. [c]Values are estimated from permeability data of a homogeneous membrane by assuming a thickness of 50 nm.

more attention from both scientific and engineering viewpoints. The membranes fabricated in this study show rather high CO_2 permeance and CO_2/N_2 selectivity, especially when the feed pressure increases up to 5 bar or higher. As suggested by Yave et al.,[46] the addition of low-molecular poly(ethylene glycol) (PEG) into the selective layer is expected to further enhance CO_2 permeance.

4. CONCLUSIONS

In this study, high-performance composite membranes were designed and fabricated following a novel strategy of enriching CO_2-philic PEO groups at the interface, which could be readily realized by surface segregation of PEO-containing block copolymers during the fabrication of a porous support layer. With a thin film of WSP as the selective layer, the composite membranes display high CO_2 permeance, high CO_2/N_2 selectivity, and high structural stability at a humidified state. PEO-enriched interfacial zone not only served to increase the preferential sorption of CO_2 but also enhanced the interfacial adhesion (confirmed by T-peel and PAS data) and stability. On the basis of the experimental results and previous literature, a picture of the desired interfacial structure of a WSP-based composite membrane for CO_2 capture was tentatively depicted. In the future, other polar groups are expected to be enriched at the interface of composite membranes by surface modification of the support layer, so as to further enhance the separation performance and interfacial stability. Also, different WSPs can be used as selective materials to investigate how the adjacent layers can be well matched.

■ ASSOCIATED CONTENT

Ⓢ Supporting Information

Gas-permeation apparatus scheme, FESEM images, FT-IR spectra, and some other supporting data for structure characterization, including the calculating method of the surface coverage of PEO, the effect of the temperature on the membrane performance, and long-term stability. This material is available free of charge via the Internet at http://pubs.acs.org.

■ AUTHOR INFORMATION

Corresponding Author

*Tel: +86 22 23500086. Fax: +86 22 23500086. E-mail: zhyjiang@tju.edu.cn.

Author Contributions

The manuscript was written through contributions of all authors. All authors have given approval to the final version of the manuscript.

Notes

The authors declare no competing financial interest.

■ ACKNOWLEDGMENTS

This study was financially supported by the National High Technology Research and Development Program of China (Grant 2012AA03A611), National Science Fund for Distinguished Young Scholars (Grant 21125627), Tianjin Natural Science Foundation (Grant 10JCZDJC22600), and Program of Introducing Talents of Discipline to Universities (Grant B06006).

■ REFERENCES

(1) Zhang, L.; Xu, N.; Li, X.; Wang, S.; Huang, K.; Harris, W. H.; Chiu, W. K. S. High CO_2 Permeation Flux Enabled by Highly Interconnected Three-Dimensional Ionic Channels in Selective CO_2 Separation Membranes. *Energy Environ. Sci.* **2012**, *5*, 8310−8317.

(2) Dawson, R.; Stockel, E.; Holst, J. R.; Adams, D. J.; Cooper, A. I. Microporous Organic Polymers for Carbon Dioxide Capture. *Energy Environ. Sci.* **2011**, *4*, 4239−4245.

(3) Sanders, D. F.; Smith, Z. P.; Guo, R.; Robeson, L. M.; McGrath, J. E.; Paul, D. R.; Freeman, B. D. Energy-Efficient Polymeric Gas Separation Membranes for a Sustainable Future: A Review. *Polymer* **2013**, *54*, 4729−4761.
(4) Du, N.; Park, H. B.; Dal-Cin, M. M.; Guiver, M. D. Advances in High Permeability Polymeric Membrane Materials for CO_2 Separations. *Energy Environ. Sci.* **2012**, *5*, 7306−7322.
(5) Li, S.; Wang, Z.; Yu, X.; Wang, J.; Wang, S. High-Performance Membranes with Multi-permselectivity for CO_2 Separation. *Adv. Mater.* **2012**, *24*, 3196−3200.
(6) Merkel, T. C.; Lin, H.; Wei, X.; Baker, R. Power Plant Post-combustion Carbon Dioxide Capture: An Opportunity for Membranes. *J. Membr. Sci.* **2010**, *359*, 126−139.
(7) Ramasubramanian, K.; Verweij, H.; Winston Ho, W. S. Membrane Processes for Carbon Capture from Coal-Fired Power Plant Flue Gas: A Modeling and Cost Study. *J. Membr. Sci.* **2012**, *421*−*422*, 299−310.
(8) Du, N.; Park, H. B.; Robertson, G. P.; Dal-Cin, M. M.; Visser, T.; Scoles, L.; Guiver, M. D. Polymer Nanosieve Membranes for CO_2-Capture Applications. *Nat. Mater.* **2011**, *10*, 372−375.
(9) Lau, C. H.; Liu, S.; Paul, D. R.; Xia, J.; Jean, Y.-C.; Chen, H.; Shao, L.; Chung, T.-S. Silica Nanohybrid Membranes with High CO_2 Affinity for Green Hydrogen Purification. *Adv. Energy Mater.* **2011**, *1*, 634−642.
(10) Park, H. B.; Jung, C. H.; Lee, Y. M.; Hill, A. J.; Pas, S. J.; Mudie, S. T.; Van Wagner, E.; Freeman, B. D.; Cookson, D. J. Polymers with Cavities Tuned for Fast Selective Transport of Small Molecules and Ions. *Science* **2007**, *318*, 254−258.
(11) Zhao, Y.; Winston Ho, W. S. Steric Hindrance Effect on Amine Demonstrated in Solid Polymer Membranes for CO_2 Transport. *J. Membr. Sci.* **2012**, *415*−*416*, 132−138.
(12) Yong, W. F.; Li, F. Y.; Xiao, Y. C.; Chung, T. S.; Tong, Y. W. High Performance PIM-1/Matrimid Hollow Fiber Membranes for CO_2/CH_4, O_2/N_2 and CO_2/N_2 Separation. *J. Membr. Sci.* **2013**, *443*, 156−169.
(13) Omole, I. C.; Adams, R. T.; Miller, S. J.; Koros, W. J. Effects of CO_2 on a High Performance hollow-fiber membrane for natural gas purification. *Ind. Eng. Chem. Res.* **2010**, *49*, 4887−4896.
(14) Sandru, M.; Haukebo, S. H.; Hagg, M. B. Composite Hollow Fiber Membranes for CO_2 Capture. *J. Membr. Sci.* **2010**, *346*, 172−186.
(15) Kim, S.; Han, S. H.; Lee, Y. M. Thermally Rearranged (TR) Polybenzoxazole Hollow Fiber Membranes for CO_2 Capture. *J. Membr. Sci.* **2012**, *403*−*404*, 169−178.
(16) Yave, W.; Car, A.; Wind, J.; Peinemann, K. V. Nanometric Thin Film Membranes Manufactured on Square Meter Scale: Ultra-thin Films for CO_2 Capture. *Nanotechnology* **2010**, *21*, 1−7.
(17) Yave, W.; Huth, H.; Car, A.; Schick, C. Peculiarity of a CO_2-philic Block Copolymer Confined in Thin Films with Constrained Thickness: "A Super Membrane for CO_2-Capture". *Energy Environ. Sci.* **2011**, *4*, 4656−4661.
(18) Blinova, N. V.; Svec, F. Functionalized Polyaniline-based Composite Membranes with Vastly Improved Performance for Separation of Carbon Dioxide from Methane. *J. Membr. Sci.* **2012**, *423*−*424*, 514−521.
(19) Zhao, J.; Wang, Z.; Wang, J.; Wang, S. High-Performance Membranes Comprising Polyaniline Nanoparticles Incorporated into Polyvinylamine Matrix for CO_2/N_2 Separation. *J. Membr. Sci.* **2012**, *403*−*404*, 203−215.
(20) Poloncarzova, M.; Vejrazka, J.; Vesely, V.; Izak, P. Effective Purification of Biogas by a Condensing-Liquid Membrane. *Angew. Chem., Int. Ed.* **2011**, *50*, 669−671.
(21) James, M.; Darwish, T. A.; Ciampi, S.; Sylvester, S. O.; Zhang, Z.; Ng, A.; Gooding, J. J.; Hanley, T. L. Nanoscale Condensation of Water on Self-assembled Monolayers. *Soft Matter* **2011**, *7*, 5309−5318.
(22) Low, B. T.; Zhao, L.; Merkel, T. C.; Weber, M.; Stolten, D. A Parametric Study of the Impact of Membrane Materials and Process Operating Conditions on Carbon Capture from Humidified Flue Gas. *J. Membr. Sci.* **2013**, *431*, 139−155.
(23) Yuan, S.; Wang, Z.; Qiao, Z.; Wang, M.; Wang, J.; Wang, S. Improvement of CO_2/N_2 Separation Characteristics of Polyvinylamine by Modifying with Ethylenediamine. *J. Membr. Sci.* **2011**, *378*, 425−437.
(24) Qiao, Z.; Wang, Z.; Zhang, C.; Yuan, S.; Zhu, Y.; Wang, J.; Wang, S. PVAm−PIP/PS Composite Membrane with High Performance for CO_2/N_2 Separation. *AIChE J.* **2013**, *59*, 215−228.
(25) Wang, M.; Wang, Z.; Li, S.; Zhang, C.; Wang, J.; Wang, S. A High Performance Antioxidative and Acid Resistant Membrane Prepared by Interfacial Polymerization for CO_2 Separation from Flue Gas. *Energy Environ. Sci.* **2013**, *6*, 539−551.
(26) Huang, J.; Zou, J.; Ho, W. S. W. Carbon Dioxide Capture Using a CO_2-Selective Facilitated Transport Nembrane. *Ind. Eng. Chem. Res.* **2008**, *47*, 1261−1267.
(27) El-Azzami, L. A.; Grulke, E. A. Carbon Dioxide Separation from Hydrogen and Nitrogen: Facilitated Transport in Arginine Salt−Chitosan Membranes. *J. Membr. Sci.* **2009**, *328*, 15−22.
(28) Shishatskiy, S.; Pauls, J. R.; Nunes, S. P.; Peinemann, K. V. Quaternary Ammonium Membrane Materials for CO_2 Separation. *J. Membr. Sci.* **2010**, *359*, 44−53.
(29) Nguyen, H. K.; Labardi, M.; Capaccioli, S.; Lucchesi, M.; Rolla, P.; Prevosto, D. Interfacial and Annealing Effects on Primary α-relaxation of Ultrathin Polymer Films Investigated at Nanoscale. *Macromolecules* **2012**, *45*, 2138−2144.
(30) Ma, J.; Zhang, M. H.; Wu, H.; Yin, X.; Chen, J.; Jiang, Z. Y. Mussel-Inspired Fabrication of Structurally Stable Chitosan/Polyacrylonitrile Composite Membrane for Pervaporation Dehydration. *J. Membr. Sci.* **2010**, *348*, 150−159.
(31) Tabor, D. Surface Forces and Surface Interactions. *J. Colloid Interface Sci.* **1977**, *58*, 2−13.
(32) Yave, W.; Szymczyk, A.; Yave, N.; Roslaniec, Z. Design, Synthesis, Characterization and Optimization of PTT-*b*-PEO Copolymers: A New Membrane Material for CO_2 Separation. *J. Membr. Sci.* **2010**, *362*, 407−416.
(33) McKeown, N. B.; Budd, P. M.; Msayib, K. J.; Ghanem, B. S.; Kingston, H. J.; Tattershall, C. E.; Makhseed, S.; Reynolds, K. J.; Fritsch, D. Polymers of Intrinsic Microporosity (PIMs): Bridging the Void Between Microporous and Polymeric Materials. *Chem.—Eur. J.* **2005**, *11*, 2610−2620.
(34) Wang, Y. Q.; Wang, T.; Su, Y. L.; Peng, F. B.; Wu, H.; Jiang, Z. Y. Remarkable Reduction of Irreversible Fouling and Improvement of the Permeation Properties of Poly(ether sulfone) Ultrafiltration Membranes by Blending with Pluronic F127. *Langmuir* **2005**, *21*, 11856−11862.
(35) Li, B.; Zhao, W.; Su, Y. L.; Jiang, Z. Y.; Dong, X.; Liu, W. P. Enhanced Desulfurization Performance and Swelling Resistance of Asymmetric Hydrophilic Pervaporation Membrane Prepared through Surface Segregation Technique. *J. Membr. Sci.* **2009**, *326*, 556−563.
(36) Zhao, X.; Su, Y.; Chen, W.; Peng, J.; Jiang, Z. pH-Responsive and Fouling-Release Properties of PES Ultrafiltration Membranes Modified by Multi-functional Block-like Copolymers. *J. Membr. Sci.* **2011**, *382*, 222−230.
(37) Shah, T. N.; Foley, H. C.; Zydney, A. L. Development and Characterization of Nanoporous Carbon Membranes for protein ultrafiltration. *J. Membr. Sci.* **2007**, *295*, 40−49.
(38) Zhao, W.; Su, Y.; Li, C.; Shi, Q.; Ning, X.; Jiang, Z. Fabrication of Antifouling Polyethersulfone Ultrafiltration Membranes Using Pluronic F127 as Both Surface Modifier and Pore-Forming Agent. *J. Membr. Sci.* **2008**, *318*, 405−412.
(39) Liu, L.; Jiang, N.; Burns, C. M.; Chakma, A.; Feng, X. S. Substrate Resistance in Composite Membranes for Organic Vapour/Gas Separations. *J. Membr. Sci.* **2009**, *338*, 153−160.
(40) Ren, X.; Ren, J.; Li, H.; Feng, S.; Deng, M. Poly(amide-6-*b*-ethylene oxide) Multilayer Composite Membrane for Carbon Dioxide Separation. *Int. J. Greenhouse Gas Control* **2012**, *8*, 111−120.
(41) Zhao, C.; Wu, H.; Li, X.; Pan, F.; Li, Y.; Zhao, J.; Jiang, Z.; Zhang, P.; Cao, X.; Wang, B. High Performance Composite Membranes with a Polycarbophil Calcium Transition Layer for

Pervaporation Dehydration of Ethanol. *J. Membr. Sci.* **2013**, *429*, 409−417.
(42) Car, A.; Stropnik, C.; Yave, W.; Peinemann, K. V. Tailor-made Polymeric Membranes Based on Segmented Block Copolymers for CO_2 Separation. *Adv. Funct. Mater.* **2008**, *18*, 2815−2823.
(43) Car, A.; Stropnik, C.; Yave, W.; Peinemann, K. V. PEG Modified Poly(amide-*b*-ethylene oxide) Membranes for CO_2 Separation. *J. Membr. Sci.* **2008**, *307*, 88−95.
(44) Yave, W.; Car, A.; Funari, S. S.; Nunes, S. P.; Peinemann, K. V. CO_2-Philic Polymer Membrane with Extremely High Separation Performance. *Macromolecules* **2010**, *43*, 326−333.
(45) Car, A.; Stropnik, C.; Yave, W.; Peinemann, K. V. Pebax (R)/Polyethylene Glycol Blend Thin Film Composite Membranes for CO_2 Separation: Performance with Mixed Gases. *Sep. Purif. Technol.* **2008**, *62*, 110−117.
(46) Yave, W.; Car, A.; Peinemann, K. V. Nanostructured Membrane Material Designed for Carbon Dioxide Separation. *J. Membr. Sci.* **2010**, *350*, 124−129.
(47) Xu, R.; Winnik, M. A.; Riess, G.; Chu, B.; Croucher, M. D. Micellization of Polystyrene−Poly(ethylene oxide) Block Copolymers in Water. 5. A Test of the Star and Mean-field Models. *Macromolecules* **1992**, *25*, 644−652.
(48) Chapman, P. D.; Oliveira, T.; Livingston, A. G.; Li, K. Membranes for the Dehydration of Solvents by Pervaporation. *J. Membr. Sci.* **2008**, *318*, 5−37.
(49) Shao, P.; Huang, R. Y. M. Polymeric Membrane Pervaporation. *J. Membr. Sci.* **2007**, *287*, 162−179.
(50) Zhao, C.; Wu, H.; Li, X.; Pan, F.; Li, Y.; Zhao, J.; Jiang, Z.; Zhang, P.; Cao, X.; Wang, B. High performance composite membranes with a polycarbophil calcium transition layer for pervaporation dehydration of ethanol. *J. Membr. Sci.* **2013**, *429*, 409−417.
(51) Wu, H.; Zhang, X. F.; Xu, D.; Li, B.; Jiang, Z. Y. Enhancing the Interfacial Stability and Solvent-Resistant Property of PDMS/PES Composite Membrane by Introducing a Bifunctional Aminosilane. *J. Membr. Sci.* **2009**, *337*, 61−69.
(52) Ma, J.; Zhang, M. H.; Jiang, Z. Y.; Nie, M. C.; Liu, G. X. Facile Fabrication of Structurally Stable Hyaluronic Acid-Based Composite Membranes Inspired by Bioadhesion. *J. Membr. Sci.* **2010**, *364*, 290−297.
(53) Dai, Y.; Johnson, J. R.; Karvan, O.; Sholl, D. S.; Koros, W. J. Ultem®/ZIF-8 Mixed Matrix Hollow Fiber Membranes for CO_2/N_2 Separations. *J. Membr. Sci.* **2012**, *401−402*, 76−82.
(54) Magueijo, V. M.; Anderson, L. G.; Fletcher, A. J.; Shilton, S. J. Polysulfone Mixed Matrix Gas Separation Hollow Fibre Membranes Filled with Polymer and Carbon Xerogels. *Chem. Eng. Sci.* **2013**, *92*, 13−20.
(55) Ji, P. F.; Cao, Y. M.; Zhao, H. Y.; Kang, G. D.; Jie, X. M.; Liu, D. D.; Liu, J. H.; Yuan, Q. Preparation of Hollow Fiber Poly(*N*,*N*-dimethylaminoethyl methacrylate)−Poly(ethylene glycol methyl ether methyl acrylate)/Polysulfone Composite Membranes for CO_2/N_2 Separation. *J. Membr. Sci.* **2009**, *342*, 190−197.